IEEE Access
Multidisciplinary | Rapid Review | Open Access Journal

Received April 1, 2018, accepted May 22, 2018, date of publication June 6, 2018, date of current version July 6, 2018.

Digital Object Identifier 10.1109/ACCESS.2018.2841988

Configuration Optimization and a Tension Distribution Algorithm for Cable-Driven Parallel Robots

DA SONG, (Student Member, IEEE), LIXUN ZHANG, AND FENG XUE
College of Mechanical and Electrical Engineering, Harbin Engineering University, Harbin 150001, China
Corresponding author: Lixun Zhang (zhanglixun@hrbeu.edu.cn)

This work was supported by the National Natural Science Foundation of China under Grant 61773007 and Grant 61175128.

ABSTRACT In order to improve the performance of cable-driven parallel robots (CDPRs), the configuration of the redundantly actuated CDPRs is optimized, and a feasible continuous tension distribution method for tracking the trajectory of the robot is proposed. A convex analysis method is used to determine the wrench-feasible workspace of CDPRs and the grouped coordinate descent method is used to determine the size of the redundantly actuated six-degree-of-freedom CDPRs. By changing the cable layout and using the geometric analysis method for the redundantly actuated CDPRs, the maximum rotation angle of the mobile platform in 3-D space is determined. The optimal size and layout of the CDPR are determined by comparison and analysis. The high dynamic CDPRs require real-time control to adjust the cable tension. In order to solve this issue, a real-time cable tension distribution algorithm for a non-iteration two-degree-of-freedom actuation redundancy CDPR is proposed. The proposed tension distribution algorithm is applied to the optimized six-degree-of-freedom eight-cable CDPR, and compared with other existing cable tension distribution algorithms. The simulation results demonstrated that the feasibility and the advantages of the proposed cable tension distribution algorithm.

INDEX TERMS Cable-driven parallel robots, cable layout, wrench-feasible workspace, tension distribution algorithm.

I. INTRODUCTION

Cable-driven parallel robots (CDPRs) components include a fixed platform, a cable drive unit, cables, and a mobile platform. For example, a typical CDPR, a cable-driven virtual assembly training robot (CDVATR), has been shown in Fig. 1. The computer control cable drive unit transmits motion and force to the mobile platform via the cables. Due to the physical characteristics of the cable, these parallel robots have several properties, such as a very large reachable workspace, high speed, large carrying capacity, low installation and maintenance costs [1]–[3]. Because of its unique advantages, CDPRs is applied in many industrial situations, e.g., rehabilitation system [4]–[6], camera robot [7], giant radio telescope [8]–[10] and haptic interfaces [11], [12], locomotion interfaces [13]. Since cables can only work in tension, i.e., the cable tension must satisfy the unidirectional force property that the tension must maintain positive, hence it needs considering the unidirectional force property under arbitrary external wrench when the mobile platform is in different

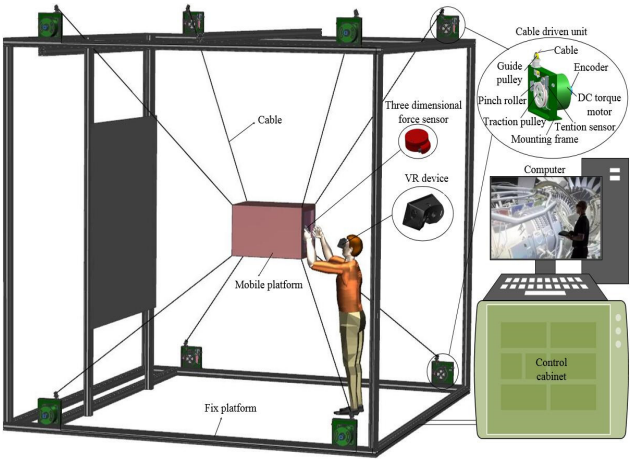

FIGURE 1. Cable-driven virtual assembly training robot.

poses [14], [15]. The unilateral nature of cable forces, CDPRs has many disadvantages, which limits its application to some extent. For example, *n*-degree-of-freedom (DOF) CDPRs

need to use at least $n + 1$ drive units to ensure that each cable maintains a positive tension. According to the relationship between the number of cable m and the number of degrees of freedom n, the general CDPRs can be divided into three types, that is, under constraint cable parallel mechanism ($m < n + 1$), completely constrained cable parallel mechanism ($m = n + 1$), redundant constraint cable parallel mechanism ($m > n + 1$) [16].

The workspace of a CDPR is one of the most important indexes for evaluating the performance of a robot. In order to improve the performance of CDPRs, many researchers have paid attention to the workspace. According to the properties of cable tension, the workspace associated with the robot structure and the mobile platform pose is defined as the wrench closed workspace [17], [18], and with the structure of the robot, the mobile platform pose and the cable tension is defined as the wrench feasible workspace (WFW) [19]–[21]. In general terms, if the mobile platform is located in the WFW, the cables within the given tension range can balance the external wrench set applied to the mobile platform [22], [23]. However, the workspace of the CDPR is also affected by cable interference. Collisions between cable and cable, and mobile platform and cable should be avoided during movement of the robots. Merlet [24] proposed an algorithm that allow to study the influence of cable and cable, and cable and mobile platform interference on the workspace, assuming a fixed orientation of the fixed platform. Blanchet [25] presented two algorithms to handle the collisions with the robot's environment and self-interference. However, there are some references that allow the collision of cable and cable in order to increase the workspace of the robot [26], but a collision between cable and cable can reduce the control accuracy or even cause loss of control of the robot. Some researchers have analyzed the influence of the cable layout on the workspace of the plane CDPR, and improved the robot workspace quality by changing the position parameters of the pulley in the fixed platform [27]–[29]. Nguyen *et al.* [30] and Nguyen and Gouttefarde [31] used multi-objective optimization to change the position of the hinge point of the cable and the fixed platform to improve the quality of the workspace of the suspension CDPR. Lorenzo Gagliardini *et al.* [32] used a Dijkstra's based algorithm to optimize the position of the hinge point of the cable and the fixed platform to expand the workspace of the CDPR. Although most of the research that is carried out on the WFW has mainly focused on the influence of the mobile platform, the fixed platform, and tension constraints there is a few references analysis of the influence of the hinge point of cable and mobile platform on the WFW. Therefore, it is necessary to study the influence of the cable layout on the WFW and the cable layout needs to be optimized.

Another restriction factor of the CDPR is that the robot needs to meet the workspace requirements and, at the same time, it must meet the stiffness variable and the corresponding speed requirements [33]. If it is to achieve real-time control. For example, the CDVATR, shown in Fig. 1, needs to be simulated to adjust the location of different size and quality objects in real time. Therefore, redundantly actuated CDPRs require a tension distribution algorithm that meets the requirements for real-time control. Some previous studies have focused on optimizing the tension distribution in the cables. In [34] and [35] put forward an objective function to optimize the cable tension distribution with p-norm. However, this method can easily cause cable tension discontinuity when the mobile platform moves along the track. In [36] presents a simple, fast, predictive computation method for a CDPR with 2-DOF or 3-DOF actuation redundancy. However, this method does not prove that the CDPR works in the WFW. Further, a general problem is that the exact solution cannot be found. In [37], a safe tension method is proposed to increase the stiffness of the CDPR to avoid low cable tension. However, a safe and reliable calculation of the cable tension distribution is time-consuming and affects the real-time performance control of the robot. In addition, the safe tension method relies on linear programming so that the cable tension calculated in the worst-case may be discontinuous. In [38]–[40] has proposed a tension optimization distribution algorithm based on obtaining the cable tension and configuring the center of gravity, which is located in the effective tension polyhedron, without iteration. This algorithm is proven to be continuous along the given trajectory. Then, this algorithm is a resource intensive computation because of the high actuation redundancy, and it takes a lot of time to compute the center of gravity of the polygon. Therefore, an algorithm is proposed to obtain tension optimization distribution without compute the center of gravity of the polygon.

Therefore, this paper has investigated the WFW algorithm considering interference, which makes the obtained workspace closer to the actual workspace of CDPRs. To maximize the WFW, the mechanical structure of a CDPM is optimized using the grouped coordinate descent (GCD) method. The workspace corresponding to the optimal size of the mobile platform is calculated by using the WFW algorithm, and the continuity of the workspace is verified. The influence of the cable layout on the WFW is further analyzed, and the maximum attitude angle of the three layout schemes is determined. Through comprehensive comparison and analysis, the optimal configuration for CDPRs is determined. Furthermore, the problem of optimal tension distribution is transformed into a convex program problem based on convex theory. Then, any point is used as the starting point to find next feasible points along the line motion to determine the feasible region. Finally, the best feasible point is quickly determine. Thus, an algorithm for optimal distribution of cable tension, which takes full account of the time when the cable tension is feasible in the feasible polygon and reduces the CDPRs energy loss, is introduced. Finally, the feasibility, continuity, and real-time performance of the algorithm are verified by simulation experiments. Compared with other algorithms proposed in references, the advantages of the proposed algorithm are further proved.

The rest of this paper is organized as follows. In section II, the kinematic and dynamic modelling of CDPRs are established. In section III, judgment conditions of WFW considering interference. In section IV, configuration optimization of CDPRs and determination of optimal configuration. In section V, a rapid optimization method of cable tension distribution is proposed, and detailed design procedures are described. In section VI, simulation experiments are implemented on a six degree of freedom eight cables CDPR, the feasibility and advantages of the proposed algorithm are analysed. Finally, concluding remarks are presented in section VII.

II. KINEMATIC AND DYNAMIC MODELING

Notation of a n-DOF CDPR with m cables is shown in Fig. 2; coordinate frame O is the base frame and coordinate frame O_1 is the local frame fixed on the mobile platform. The kinematic and dynamic equations of a CDPR can be derived based on the architecture shown in Fig. 2. Here, the gravity of the cable is neglected, and each cable is considered a straight line.

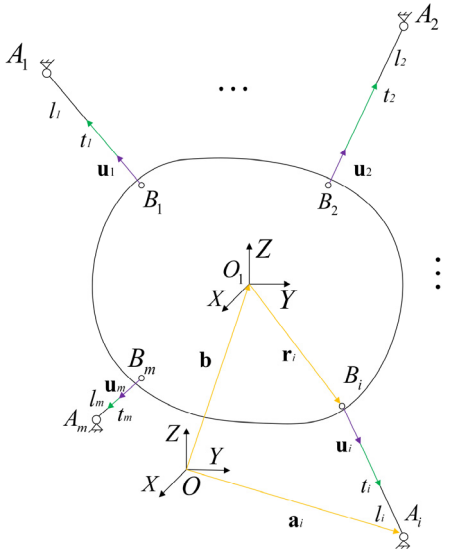

FIGURE 2. Notation of an n-DOF CDPR.

A. KINEMATIC MODELING

The position of the connection point between the guide pulley and the cable of the drive unit is expressed as A_i in the coordinate frame O, and vector $\mathbf{a}_i$ are constant position vectors connecting O to A_i. The coordinate frame O_1 is expressed as $\mathbf{b}$ in the coordinate frame O. The position vector of hinge point location B_i on mobile platform and point B_i in the local frame O_1 representations for $\mathbf{r}_i$. The Z-Y-X Euler angles of the local frame to the base frame are α, β, γ, and the corresponding coordinate frame based on mobile platform for attitude angles is (α, β, γ). $\mathbf{R}$ is the transformation matrix from O_1 to O which is expressed in (1), as shown at the bottom of this page.

The kinematic of each cable can be established by the vector loop method:

$$\mathbf{l}_i = \mathbf{a}_i - (\mathbf{b} + {}^{O}\mathbf{R}_{O_1}\mathbf{r}_i) \quad i = 1, 2, \cdots, m \tag{2}$$

Then, the unit vector of the ith cable becomes:

$$\mathbf{u}_i = \mathbf{l}_i / \parallel \mathbf{l}_i \parallel \quad i = 1, 2, \cdots, m \tag{3}$$

B. DYNAMIC MODELING

Assume that the cable mass of the CDPR can be very small, and its gravity and inertia force can be neglected during moving. However, in general, the quality of the mobile platform is very high, and there may be large speed and acceleration while moving. Therefore, the gravity and inertia of the mobile platform cannot be ignored. According to Newton's law, the dynamic model of the CDPR is obtained:

$$\mathbf{JT} + \mathbf{G} + \mathbf{W} = \mathbf{M}\ddot{\mathbf{X}} + \mathbf{N}\dot{\mathbf{X}} \tag{4}$$

where

$$\mathbf{J} = \begin{bmatrix} \mathbf{u}_1 & \mathbf{u}_2 & \cdots & \mathbf{u}_m \\ \mathbf{r}_1 \times \mathbf{u}_1 & \mathbf{r}_2 \times \mathbf{u}_2 & \cdots & \mathbf{r}_m \times \mathbf{u}_m \end{bmatrix},$$

$$\mathbf{T} = [t_1 \quad t_2 \quad \cdots \quad t_m]^T$$

$$\mathbf{G} = [m\mathbf{g} \quad c \times m\mathbf{g}]^T, \quad \mathbf{W} = \begin{bmatrix} F_x & F_y & F_z & M_x & M_y & M_z \end{bmatrix}^T$$

$$\mathbf{M} = \begin{bmatrix} m\begin{bmatrix} 1 & 0 & 0 \\ 0 & 1 & 0 \\ 0 & 0 & 1 \end{bmatrix} & -m\begin{bmatrix} 0 & -c_z & c_y \\ c_z & 0 & -c_x \\ -c_y & -c_x & 0 \end{bmatrix} \\ m\begin{bmatrix} 0 & -c_z & c_y \\ c_z & 0 & -c_x \\ -c_y & -c_x & 0 \end{bmatrix} & \begin{bmatrix} I_{xx} & -I_{xy} & -I_{xz} \\ -I_{yx} & I_{yy} & -I_{yz} \\ -I_{zx} & -I_{zy} & I_{zz} \end{bmatrix} \end{bmatrix}$$

$$\mathbf{I}_{O_1} = \begin{bmatrix} I_{xx} & -I_{xy} & -I_{xz} \\ -I_{yx} & I_{yy} & -I_{yz} \\ -I_{zx} & -I_{zy} & I_{zz} \end{bmatrix}, \quad \mathbf{c} = \begin{bmatrix} 0 & -c_z & c_y \\ c_z & 0 & -c_x \\ -c_y & -c_x & 0 \end{bmatrix}$$

$$\mathbf{X} = [x \quad y \quad z \quad \alpha \quad \beta \quad \gamma]^T,$$

$$\mathbf{N} = \begin{bmatrix} \mathbf{0} & -m(w \times \mathbf{c})^{\times} \\ m(w \times \mathbf{c})^{\times} & -(\mathbf{I}_{O_1} w)^{\times} \end{bmatrix}$$

In the above equations, vectors $\mathbf{G} \in \mathbf{R}^6$ and $\mathbf{W} \in \mathbf{R}^6$ are the gravity wrench and the external wrench, respectively; m is the mass of the mobile platform; $\mathbf{I}_{O_1}$ is the 3×3 inertia tensor of the mobile platform about applied point of external wrench; $\mathbf{g} \in \mathbf{R}^3$ is the gravity acceleration vector; $\mathbf{T} \in \mathbf{R}^m$ is a vector consisting of all individual cable forces; t_i is the cable force of the ith cable; $\mathbf{J}$ is the 6×m Jacobian matric of the CDPR;

$${}^{O}\mathbf{R}_{O_1} = \begin{bmatrix} \cos\alpha\cos\beta & \cos\alpha\sin\beta\sin\gamma - \sin\alpha\cos\gamma & \cos\alpha\sin\beta\cos\gamma + \sin\alpha\sin\gamma \\ \sin\alpha\cos\beta & \sin\alpha\sin\beta\sin\gamma + \cos\alpha\cos\gamma & \sin\alpha\sin\beta\cos\gamma - \cos\alpha\sin\gamma \\ -\sin\beta & \cos\beta\sin\gamma & \cos\beta\cos\gamma \end{bmatrix} \tag{1}$$

$\mathbf{c} \in \mathbf{R}^3$ is the position vector of the mass center of the mobile platform in the O_1 coordinate frame.

Let $\mathbf{W}_e = \mathbf{M}\ddot{\mathbf{X}} + \mathbf{V}\dot{\mathbf{X}} - \mathbf{G} - \mathbf{W}$. Then, the Eq. (4) can be re-written into a compact form as:

$$\mathbf{JT} = \mathbf{W}_e \tag{5}$$

III. WFW ANALYSIS

The accurate judgment of the WFW of a CDPR lays a theoretical foundation for the trajectory planning and control of the robot. In addition to meeting the WFW, the robot needs to determine whether there is interference between cable and cable, and cable and the mobile platform, so that the robot will not lose control or damage during the movement process.

A. WFW DEFINITION

Definition 1: The WFW is the set of mobile platform poses that are wrench-feasible, i.e., for which, for any wrench $\mathbf{W}_e$ in $\mathbf{W}_T$, there exists a vector of cable tension $\mathbf{T}$ in $\mathbf{T}_{req} = \{t | t_i \in [t_{\min}, t_{\max}], 1 \le i \le m\}$ such that $\mathbf{JT} = \mathbf{W}_e$ [23].

The WFW needs to be satisfied with the conditions defined as the balance of the cable tension for a given range of external wrench in a certain range [41]. Expression as:

$$\forall \mathbf{W}_e \in \mathbf{W}_T \quad \forall \mathbf{T} \in \mathbf{T}_{req} \quad \mathbf{JT} = \mathbf{W}_e \tag{6}$$

where $\mathbf{W}_T$, $\mathbf{T}_{req}$ is the set of external wrench and the cable tension set to meet the requirements, respectively.

$$\mathbf{\Gamma} = \{\mathbf{W}_T \mid w_d \in [w_{\min}, w_{\max}], \ 1 \le d \le n\} \tag{7}$$

$$\mathbf{\Omega} = \left\{\mathbf{T}_{req} \mid t_i \in [t_{\min}, t_{\max}], \ 1 \le i \le m\right\} \tag{8}$$

where $w_{\min}$, $w_{\max}$ are the minimum and maximum of the external wrench, respectively. $t_{\min}$, $t_{\max}$ are the minimum and maximum of each cable tension, respectively.

According to the wrench feasible condition definition, if $\mathbf{W}_A = \left\{\mathbf{JT} \middle| \mathbf{T} \in \mathbf{T}_{req}\right\}$ and $\mathbf{W}_A \in \mathbf{W}_T$ are set up, the posture of the mobile platform satisfies the wrench feasible condition. $\mathbf{W}_A$ is a convex set because $\mathbf{T}_{req}$ is a convex set [42].

B. INTERFERENCE DETECTION

When the mobile platform is moved in a certain position, it is necessary to compute the distance between the two vertical lines of the cable space and whether d is smaller than the interference threshold δ when judging whether the cables cause interference [43], [44]. As shown in Fig. 3, the cable B_iA_i and the cable B_jA_j of a CDPR can be selected as the research objects without losing its generality. The unit vector of the cable B_iA_i is $\mathbf{u}_i = (u_{ix}, u_{iy}, u_{iz})$, the plane is represented as abn_i; The unit vector of the cable B_jA_j is $\mathbf{u}_j = (u_{jx}, u_{jy}, u_{jz})$, the plane is represented as abn_j; The common normal vector between the two cables is $\mathbf{n}$=$abn_i \cap abn_j$; The unit vector of $\mathbf{n}$ is ${}^o\mathbf{n} = ({}^on_x \ {}^on_y \ {}^on_z)$, the normal vector $\mathbf{n}_i = (n_{ix}, n_{iy}, n_{iz})$ of the plane abn_i; The normal vector $\mathbf{n}_j = (n_{jx}, n_{jy}, n_{jz})$ of the plane abn_j.

From Fig. 3, it can be seen that the shortest distance between two cables is the distance between the intersection

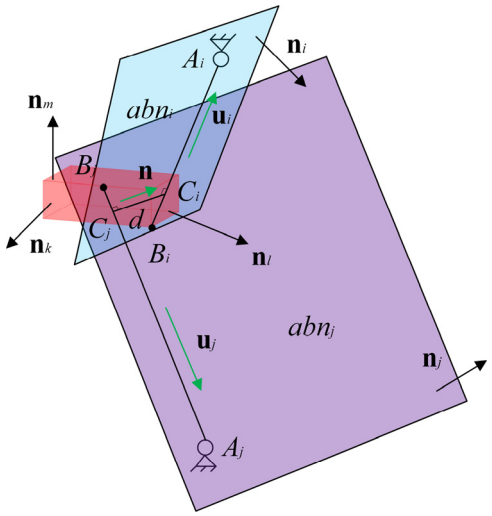

FIGURE 3. The distance between cable and cable, the angle between cable and the normal of mobile platform surface.

point C_i of the cable B_iA_i and the plane abn_i and the intersection point C_j of the cable B_jA_j and the plane abn_j. Suppose that any point on the plane abn_i is expressed as (X_i, Y_i, Z_i), and any point on the plane abn_j is expressed as (X_j, Y_j, Z_j), the two planes can be expressed by the following equations:

$$\begin{cases} n_{ix}(X_i - B_{ix}) + n_{iy}(Y_i - B_{iy}) + n_{iz}(Z_i - B_{iz}) = 0 \\ n_{jx}(X_j - B_{jx}) + n_{jy}(Y_j - B_{jy}) + n_{jz}(Z_j - B_{jz}) = 0 \end{cases} \tag{9}$$

Since points C_i and C_j, respectively, are in the cable B_iA_i and B_jA_j, the coordinates can be represented respectively as:

$$\begin{cases} C_{ix} = (B_{ix} + u_{ix}\kappa) \\ C_{iy} = (B_{iy} + u_{iy}\kappa) \\ C_{iz} = (B_{iz} + u_{iz}\kappa) \end{cases} \tag{10}$$

$$\begin{cases} C_{jx} = (B_{jx} + u_{jx}\eta) \\ C_{jy} = (B_{jy} + u_{jy}\eta) \\ C_{jz} = (B_{jz} + u_{jz}\eta) \end{cases} \tag{11}$$

Point C_i and C_j are in the plane abn_i and abn_j, by substituting (10) and (11) into (9), the proportional parameter κ, η can be obtained. Hence, the point C_i and C_j can be expressed as:

$$\begin{cases} C_{ix} = B_{ix} - u_{ix}\dfrac{n_{jx}(B_{ix}-B_{jx}) + n_{jy}(B_{iy}-B_{jy}) + n_{jz}(B_{iz}-B_{jz})}{n_{jx}u_{ix} + n_{jy}u_{iy} + n_{jz}u_{iz}} \\ C_{iy} = B_{iy} - u_{iy}\dfrac{n_{jx}(B_{ix}-B_{jx}) + n_{jy}(B_{iy}-B_{jy}) + n_{jz}(B_{iz}-B_{jz})}{n_{jx}u_{ix} + n_{jy}u_{iy} + n_{jz}u_{iz}} \\ C_{iz} = B_{iz} - u_{iz}\dfrac{n_{jx}(B_{ix}-B_{jx}) + n_{jy}(B_{iy}-B_{jy}) + n_{jz}(B_{iz}-B_{jz})}{n_{jx}u_{ix} + n_{jy}u_{iy} + n_{jz}u_{iz}} \end{cases} \tag{12}$$

$$\begin{cases} C_{jx} = B_{jx} - u_{jx}\dfrac{n_{ix}(B_{ix}-B_{jx}) + n_{iy}(B_{iy}-B_{jy}) + n_{iz}(B_{iz}-B_{jz})}{n_{ix}u_{jx} + n_{iy}u_{jy} + n_{iz}u_{jz}} \\ C_{jy} = B_{jy} - u_{jy}\dfrac{n_{ix}(B_{ix}-B_{jx}) + n_{iy}(B_{iy}-B_{jy}) + n_{iz}(B_{iz}-B_{jz})}{n_{ix}u_{jx} + n_{iy}u_{jy} + n_{iz}u_{jz}} \\ C_{jz} = B_{jz} - u_{jz}\dfrac{n_{ix}(B_{ix}-B_{jx}) + n_{iy}(B_{iy}-B_{jy}) + n_{iz}(B_{iz}-B_{jz})}{n_{ix}u_{jx} + n_{iy}u_{jy} + n_{iz}u_{jz}} \end{cases} \tag{13}$$

The distance between two points according to the distance formula between two points in space can be found using:

$$d = \left\| C_i C_j \right\|_2 \leq \delta \tag{14}$$

where δ is interference threshold, and δ cannot be zero because transversal vibration occurs when the platform moves.

The following theorem can be used to judge whether the cable interferes with the surface of the mobile platform.

Theorem 1: The mobile platform is a convex polyhedron and the surface is plane, and there is no interference between cable and plane. Only the cable unit vector and the normal vector of the hinge plane have an acute angle [43].

As shown in Fig. 3, the mobile platform is convex. The condition that the jth cable does not contact with several adjacent surfaces is given by:

$$\begin{aligned} &\arccos(u_j \cdot n_k) < 90^\circ \\ \text{or } &\arccos(u_j \cdot n_m) < 90^\circ \end{aligned} \tag{15}$$

C. SOLVING STEPS OF THE WFW WHEN CONSIDERING INTERFERENCE

According to the judgment method of the WFW that is put forward in [41] and [45], for further consideration of interference detection between cable and cable, and cable and the mobile platform, the solving steps of the WFW has more practical significance when considering the interference of the cable.

1) Set the position of the mobile platform and select the search range.

2) Determine the point of the centroid of the mobile platform, whether it meets the condition of the WFW, and determine whether there is interference between cable and cable, and cable and the mobile platform.

3) Detect whether other location points in the workspace determined by the first step, meet the WFW and interference conditions. If two judgment conditions are met at the same time then the location point is saved, if any one of them is not satisfied, the point is deleted.

Finally, the WFW, considering the interference, is finally determined. By changing the posture of the mobile platform and repeating the above process, it can be used to judge the WFW in the different postures of CDPRs.

IV. CONFIGURATION OPTIMIZATION OF CDPMs

Because of the cable's unilateral characteristics, the fixed platform and the mobile platform's size and layout will affect the workspace of the robot; therefore it is necessary to design a suitable fixed platform and mobile platform size and layout of the CDPR so it has the largest WFW. Many researchers have taken a strong interest in the box structure of both fixed and mobile platform, as shown in Fig. 1. The redundant cable CDPR with a box structure improved the reliability of the robot, and at the same time, the geometric structure and the workspace are symmetrical [46]–[48]. Thus, the research work in this paper has also aimed to study a box-shaped CDPR. Fig. 1 shows a CDVATR as an example design of the size of a CDPR. Because the virtual assembly process is a human-machine interaction process, the fixed platform and mobile platform must have driving units, sensor installation dimensions, and man-machine operation. So the fixed platform side length is chosen as $\rho = 4$ m with the mobile platform as a cube of size (L_m, W_m, H_m).

A. SIZE OPTIMIZATION OF THE MOBILE PLATFORM

As shown in Fig. 1, a virtual assembly operation with a CDPR needs to meet the virtual assembly requirements of the virtual components of different spatial structures. The robot's moving space enables the robot to complete the assembly needs of larger structural components, thus making the robot more widely useable. Scheme 1 of the CDPR cable layout structure diagram of the CDVATR is shown in Fig. 4, the guide pulley of the drive unit is simplified at the apex of the fixed platform. The fixed platform is a cube of length $\rho = 4$ m. The mobile platform is a $L_m \times W_m \times H_m$ block whose center of mass is at its geometric center. The minimum tension of the cable is set to 10 N and the maximum tension is 300 N to ensure the tension of each cable.

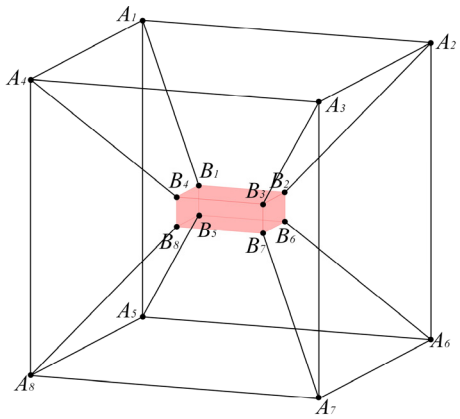

FIGURE 4. Scheme 1 CDPR cable layout structure diagram.

According to the Jacobian matrix $\mathbf{J}$, it can be known that the larger the size of the mobile platform, the larger the external force of the robot that can be balanced. However, if the size of the mobile platform is too large, it will also reduce the workspace of the robot. When keeping the mobile platform at a neutral orientation, the cable interference is the smallest and the workspace is the largest. The structure of the CDPR is optimized, and the maximum of the WFW as the objective function. As shown in Fig. 4, it is assumed that the function of the WFW of a CDPR $\mathbf{V}$ (L_m, W_m, H_m, ρ) is feasible, where L_m represents the distance of B_7B_8, W_m represents the distance of B_6B_7, and H_m represents the distance of B_3B_7. The position of the articulated point of the cable and the mobile platform can be changed arbitrarily, for example, the actual map of the virtual assembly robot.

Thus the optimization of a CDPR can be given in the form of the following expression [41]:

$$\begin{aligned} &\max\ \mathbf{V}(L_m, W_m, H_m, \rho) \\ &s.t.\ 0 \le L_m \le \rho, \quad 0 \le W_m \le \rho,\ 0 \le H_m \le \rho \end{aligned} \tag{16}$$

Although the volume of the WFW is difficult to express, the GCD method can be actually used to optimize the size of the mobile platform. Two of three unknowns, the change of one of the unknowns, which optimizes each unknowns, and the optimization process can be expressed as:

$$a^{k+1} = \arg\max_{a}\ \mathbf{V}(b, c) \tag{17}$$

where for a, b, c, if one of them represents the length variable of the mobile platform, then the other two will be expressed as width and height variables, respectively.

The size optimization of the mobile platform process is implemented in MATLAB with Intel Core i5-3470, 3.2 GHz, and 16G RAM. The algorithm proposed in part III is used to compute the WFW of the robot, and the mobile platform is searched with a search step of 0.12 m in the fixed platform space. When the size of the mobile platform is (1.2 m, 0.8 m, 0.4 m), the WFW of the robot is the largest.

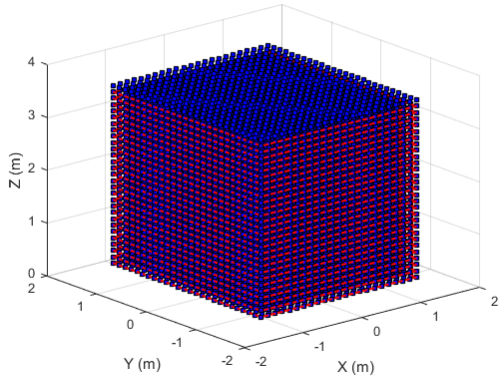

FIGURE 5. Scheme 1 optimal dimension WFW for mobile platform.

As shown in Fig. 5, the maximum number of robot workspace points is 17342. The blue box represents the workable points of the mobile platform in the fixed platform, and the red represents the boundary lines of the workspace.

B. NEW LAYOUT SCHEME

In Section IV-A determined the size of the mobile platform when the cable driven parallel machine has the maximum WFW, but at this point, the cable layout plan does not guarantee that the robot has the largest attitude angle. Therefore, it is necessary to further analyze the layout of the robot cables, and put forward second and third layout schemes, as shown in Fig. 6. As shown in Fig. 1, the CDPR needs to have the largest possible space angle in the center of the fixed platform, in order to meet different training needs. As shown in the two new layout schemes, the position of the hinge point of the cable and the mobile platform is determined by using the GCD method for the two new schemes.

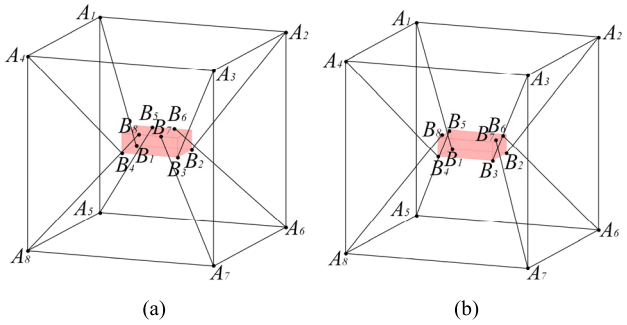

FIGURE 6. Scheme 2 and scheme 3 CDPR cable layout structure diagram, (a) represents the scheme 2, (b) represents the scheme 3.

In order to ensure the stability of the mobile platform, the position of the B_1, B_2, B_3, B_4 hinge joint is fixed because scheme 2 and scheme 3 are completely symmetrical. The GCD method in IV-A is used to optimize scheme 2 and scheme 3, and to determine the optimal distance between the hinged points B_5 and B_6, B_6 and B_7 of the cable and the mobile platform. Considering the influence of stiffness, interference, and reducing machine freedom, the distance between $B_5B_6/2$ and $B_6B_7/2$ is symmetrical, the minimum distance is 0.05 m, and the maximum distance is 0.35 m. The volume of the WFW for the different distance $B_5B_6/2$ and $B_6B_7/2$ are given in Table 1 and Table 2 which represent the number of poses within the workspace, respectively.

TABLE 1. Volume of the WFW with different distance $B_5B_6/2$.

B_5B_6 (m)	0.05	0.1	0.15	0.2	0.25	0.3	0.35
Volume	14768	15184	15635	16068	16050	16031	16028

TABLE 2. Volume of the WFW with different distance $B_6B_7/2$.

B_6B_7 (m)	0.05	0.1	0.15	0.2	0.25	0.3	0.35
Volume	14927	15526	16262	16860	17597	17242	17129

From the optimization results that are shown in Table 1, it can be seen that the optimal value of $B_5B_6/2$ is 0.2 m. From Table 2, the optimal value of $B_6B_7/2$ is 0.25 m. The optimal layout scheme for scheme 2 and scheme 3 has therefore been determined.

C. DETERMINE THE MAXIMUM ANGLE OF THE THREE SCHEMES

According to some training subjects (for example, the switch door training of the aircraft), the CDPR is required to have a large rotation angle in the centroid of the workspace. Because of the complex influences, and the three-dimensional relationship between the dimension parameters of the mobile

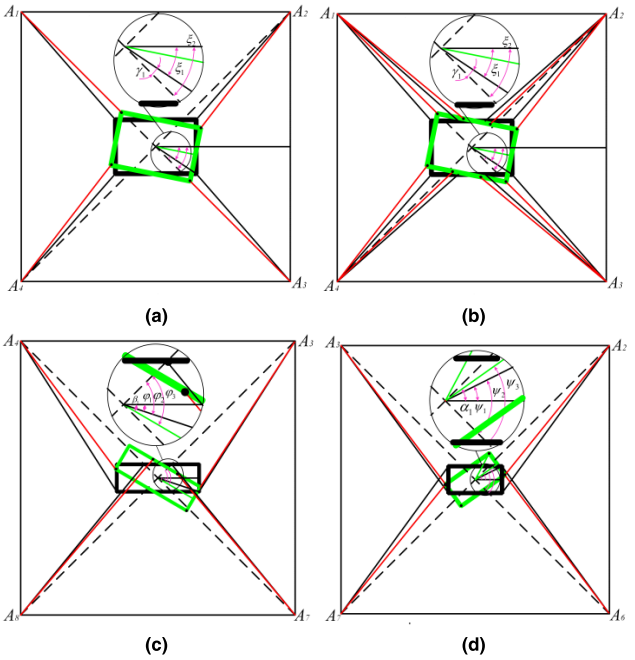

FIGURE 7. Scheme 1 and scheme 2 projection views in three directions, the wide black solid line represents the initial position of the mobile platform, and the wide green line represents the extreme position of the mobile platform that can be rotated. (a) Top view of scheme 1. (b) Top view of scheme 2. (c) Left view of scheme 2. (d) main view of scheme 2.

platform, the rotation angle is difficult to ascertain. In order to reduce the difficulty of analyzing the rotation angle in the center of the robot, the three schemes are projected onto three directions of three views, the main view, the top view and the left view, according to the geometric relationship of the fixed platform, the cable, and the mobile platform in projection view. For scheme 1 the structure of the CDPR is completely symmetrical and the projection view is the same, as shown in Fig. 7(a). From this the projection geometry relationship in the center of the robot can be established. According to the top view in Fig. 7(a), the maximum rotation angle for the three directions of the mobile platform can be obtained by:

$$\alpha_1 = \xi_2 - \xi_1 \tag{18}$$

where

$$\tan\xi_2 = 1, \quad \tan\xi_1 = \frac{W_m}{L_m}$$

According to the size of the mobile platform, determined in Section IV-A, the maximum value of the rotation angle of scheme 1 for the mobile platform in the three directions is $\alpha_1 = 11.31°$.

The geometric relationship of the rotation angle can be determined by the projection of the three directions of the scheme 2 for the mobile platform in the three directions, as shown in Fig. 7(b)–(d). According to the left view in Fig. 7(d), the angle relation can be determined as follows:

$$\gamma_1 = \psi_1 + (\psi_3 - \psi_2) \tag{19}$$

where

$$\tan\psi_1 = \frac{\frac{1}{2}H_m}{\frac{1}{2}W_m}$$

$$\cos\psi_2 = \frac{\left[\frac{1}{2}\sqrt{H_m^2+W_m^2}\right]^2 + (\frac{\sqrt{2}}{2}l)^2 - [\sqrt{(\frac{1}{2}W_m - \frac{l}{2})^2 + (\frac{l}{2}+\frac{1}{2}H_m)^2}]^2}{\frac{\sqrt{2}}{2}l\sqrt{H_m^2+W_m^2}}$$

$$\cos\psi_3 = \frac{W_m}{l\sqrt{2}}$$

According to the main view of Fig. 7(c), the angle relation can be determined as follows:

$$\beta_1 = \varphi_1 + (\varphi_3 - \varphi_2) \tag{20}$$

where

$$\tan\varphi_1 = \frac{\frac{1}{2}H_m}{\frac{1}{2}L_m}$$

$$\cos\varphi_2 = \frac{\left[\frac{1}{2}\sqrt{L_m^2+H_m^2}\right]^2 + (\frac{\sqrt{2}}{2}l)^2 - [\sqrt{(\frac{1}{2}L_m - \frac{l}{2})^2 + (\frac{l}{2}+\frac{1}{2}H_m)^2}]^2}{\frac{\sqrt{2}}{2}l\sqrt{L_m^2+H_m^2}}$$

$$\cos\varphi_3 = \frac{L_m}{l\sqrt{2}}$$

According to the top view in Fig. 7(b), the angle relation can be determined as follows:

$$\alpha_1 = \xi_2 - \xi_1 \tag{21}$$

where

$$\tan\xi_2 = 1$$
$$\tan\xi_1 = \frac{W_m}{L_m}$$

According to the size of the mobile platform, determined in Section IV-B, the maximum value of the rotation angle of scheme 2 for the mobile platform in the three directions is $\gamma_1 = 36.87°$, $\beta_1 = 32.75°$, $\alpha_1 = 11.31°$. Scheme 3 has the same projection geometry as that of scheme 2, and the main view and left view in scheme 3 are equivalent to the scheme 2 left view and the main view respectively for the geometric relationship. Therefore, it is possible to determine that for scheme 3, $\alpha_1 = 11.31°$, $\beta_1 = 30.05°$, $\gamma_1 = 31.26°$.

By comparing the WFW of the three schemes, we know that the WFW of scheme 1 is larger than the latter two schemes, but its space rotation angle is smaller than that of the latter two schemes. The WFW of scheme 3 is larger than that of scheme 2, but the angle of space rotation is less than that of scheme 2. According to the actual application of the CDPM, scheme 2 is the best scheme for the virtual assembly training robot. The WFW range of scheme 2 is shown in Fig. 8.

From Fig. 8, the WFW of scheme 2 has more workspace in the lower half. Therefore, when designing the trajectory of the robot, we can make the trajectory in the lower half plane cover as much as possible, so that it can complete more complex virtual assembly training.

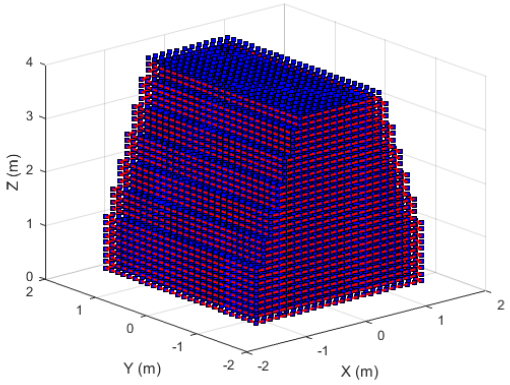

FIGURE 8. Scheme 2 optimal dimension WFW for mobile platform.

V. TENSION DISTRIBUTION ALGORITHM

Generally, 8 cable 6-DOF CDPRs with cable is redundant actuation, and the cable tension needs to be distribution in real time. Therefore, the non-iterative real-time tension distribution algorithm is necessary. For redundant actuated CDPRs, the Jacobian matrix $\mathbf{J}$ is non-square, so there are infinite solutions to the cable tension. Therefore, the real-time and rationality of the tension distribution when computing the cable tension of the CDPRs must be determined.

A. DETERMINATION OF FEASIBLE CABLE TENSION POLYGON

m cable drive units are used to control the mobile platform to make it have n-DOF and the degree of actuation redundancy is $r = m - n$. This paper studies the 8 cable CDPR with 6-DOF, so the redundant freedom degrees $r = 2$, and $\mathbf{J}$ is the 6×8 Jacobian matric. Because $\mathbf{J}$ is non-square matrix, the Moore–Penrose pseudoinverse $\mathbf{J}^+$ that needs to be introduced for calculating the cable tensions $\mathbf{T} = [t_1, \cdots, t_8] \in \mathbf{R}^8$, and the solution of the cable tensions equation is expressed as [30]:

$$\mathbf{T} = \mathbf{J}^+\mathbf{W}_e + \mathbf{N}\,\boldsymbol{\lambda} = \mathbf{T}_s + \mathbf{T}_h \tag{22}$$

with

$$\mathbf{T}_s = \mathbf{J}^+\left(\mathbf{M}\ddot{\mathbf{X}} + \mathbf{V}\dot{\mathbf{X}} - \mathbf{G} - \mathbf{W}\right) \tag{23}$$

and

$$\mathbf{T}_h = \mathbf{N}\boldsymbol{\lambda} \tag{24}$$

where $\mathbf{N}$=null($\mathbf{J}$) is a full-rank 8×2 matrix, and $\boldsymbol{\lambda} = [\lambda_1, \lambda_2]^T$ is an arbitrary 2-dimensional vector. The two columns of $\mathbf{N}$ form an orthonormal basis of the 2-dimensional nullspace of $\mathbf{J}$. $\mathbf{T}_s = \mathbf{J}^+\ \mathbf{W}_e$ is special solution to the cable tensions used to balance the external wrench on the mobile platform. $\mathbf{T}_h = \mathbf{N}\lambda$ is the homogeneous solution to the cable tensions used to regulate the internal tensions of the cable where $\mathbf{N}$ maps λ into the nullspace of $\mathbf{J}$.

Define $\boldsymbol{\Sigma} \subset \mathbf{R}^8$ the 2-dimensional affine space of the solution to (5) and $\boldsymbol{\Omega} \subset \mathbf{R}^8$ the 8-dimensional hypercube of feasible cable tensions [31]:

$$\begin{cases} \boldsymbol{\Sigma} = \{\mathbf{T} \mid \mathbf{J}\mathbf{T} = \mathbf{W}_e\} \\ \boldsymbol{\Omega} = \{\mathbf{T} \mid t_i \in [t_{\min}, t_{\max}],\ 1 \le i \le 8\} \end{cases} \tag{25}$$

Suppose that the minimum force of the 8 cable is t_{min}, and the maximum force is t_{max}. The intersection $\boldsymbol{\Lambda} = \boldsymbol{\Omega} \cap \boldsymbol{\Sigma}$ of the hypercube $\boldsymbol{\Omega}$ and the affine space $\boldsymbol{\Sigma}$ is a convex polytope representing the set of feasible tension distributions $\mathbf{T}$ [38], [39]. The preimage of is $\boldsymbol{\Lambda}$ a 2-D convex polygon; Fig. 9 shows the polygon of the CDVATR in a fixed posture.

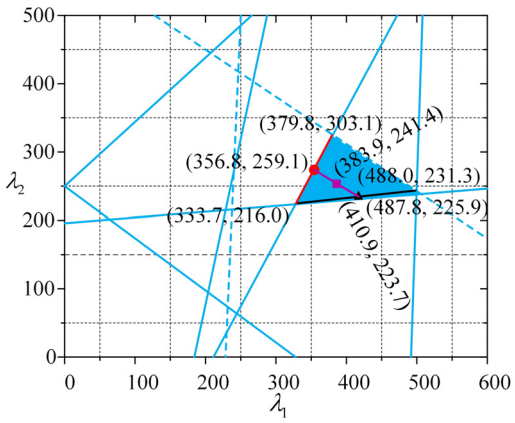

FIGURE 9. Preimage of Λ in the plane (λ_1, λ_2) for the pose (0.152, 0.254, 2.485, 0, 0, 0)^T (units: meters and degrees, *XYZ* Eurler angle convention) with a 40 kg total mass.

According to Eq. (22), the feasible polygon consists of the following 16 linear inequalities:

$$\mathbf{t}_{\min} - \mathbf{T}_s \le \mathbf{N}\,\boldsymbol{\lambda} \le \mathbf{t}_{\max} - \mathbf{T}_s \tag{26}$$

At present, there is little references on the tension polygon for the formation of the preimage of $\boldsymbol{\Lambda}$. In previous studies, the computation of the safe and continuous cable tension requires the calculating the tension feasible polygon gravity center for the formation of the preimage of $\boldsymbol{\Lambda}$ [42]. The result is safe because the feasible point selected in the feasible polygon is far away from the boundary. But this method needs to compute all the intersections in the preimage of $\boldsymbol{\Lambda}$. The preimage of $\boldsymbol{\Lambda}$ needs to compute the intersection points of any two inequality lines in Eq. (26). Eq. (26) has 2×8 inequalities; when inequality takes equal sign, each row of equation is defined as two parallel lines. Therefore, all inequalities need to be solved by solving $C_2^{16} - 8 = 112$ intersection points [38]. It is necessary to determine the center of gravity of a polygon according to the triangle method after knowing the intersection point of the feasible polygon. Although these steps are simple, computation is very time-consuming.

Hiller *et al.* [49] proposed an effective method to quickly find the intersection vertices of feasible polygons to reduce the time consumption of finding the feasible polygon vertices. The main idea of this method is to find the first intersection vertex of the preimage of $\boldsymbol{\Lambda}$, and then move along one of the lines forming the intersection point until the next new

intersection vertex is found. It is found that the process of intersection is continuous until the intersection vertices of all feasible polygon are found. The following Section V-B of simple recall step 1 and step 2, focuses on the third step, innovative methods to reduce computational feasibility polygon internal feasible point time.

B. DETERMINATION OF FEASIBLE CABLE TENSION POLYGON

The three centering method develops according to the following steps:

1) Determine any point in the preimage of $\mathbf{\Lambda}$ as the first vertex.

The symbol of inequality in Eq. (26) is replaced by an equality symbol, and the linear equations L_{ib} and L_{jb}, $\{i, j\} \in \{1, \cdots, 8\}$, $i \neq j$, which are composed of the minimum or the maximum value, are selected in any two rows of them. L_{ib} and L_{jb} constitute the first vertex $\mathbf{v}_{ij}$, and must satisfy the following conditions [50]:

$$\begin{cases} b_i - t_{si} = \mathbf{n}_i \boldsymbol{\lambda}_{ij} \\ b_j - t_{sj} = \mathbf{n}_j \boldsymbol{\lambda}_{ij} \\ \mathbf{t}_{\min} - \mathbf{T}_s \leq \mathbf{N}\lambda_{ij} \leq \mathbf{t}_{\max} - \mathbf{T}_s \end{cases} \tag{27}$$

where the 2-dimensional line vectors $\mathbf{n}_i$ and $\mathbf{n}_j$ denote the lines i and j of $\mathbf{N}$, respectively. The intersection point λ_{ij} between L_{ib} and L_{jb} is a vertex $\mathbf{v}_{ij}$ of the preimage of $\mathbf{\Lambda}$.

2) Move along one straight line.

The second step is to follow a line L_{ib} or L_{jb} along the first intersection vertex $\mathbf{v}_{ij}$, until the next intersection points $\mathbf{p}$ are found. The next points $\mathbf{p}$ determines the formula as follows:

$$\mathbf{p} = \mathbf{v}_{ij} + \alpha\ \mathbf{n}_{i\perp}^T \tag{28}$$

where $\mathbf{n}_i \mathbf{n}_{i\perp}^T = 0, \alpha$ is a scalar and its determination is detailed in [51]. After successive processes, all intersections of the final feasible polygon are determined.

3) Feasible point determination in feasible polygon.

After the first two steps, the boundary line of the convex set $\mathbf{S}$ and the intersection point $\mathbf{v}_{ij} = [v_{p_1}\ v_{p_2}]$ of the convex set are determined. According to definition:

Definition 2: $\mathbf{S} \in \mathbf{R}^n$ is a convex set, if any two points $\mathbf{v}_1$ and $\mathbf{v}_2$ in $\mathbf{S}$, arbitrary scalar $\zeta \in (0, 1)$ satisfies:

$$\zeta \mathbf{v}_1 + (1 - \zeta)\mathbf{v}_2 \in \mathbf{S} \tag{29}$$

Select the minimum point of λ_1 in the preimage of $\mathbf{\Lambda}$ as $\mathbf{v}_{\min \lambda_1} = (v_{p_{\min \lambda_1}}, v_{p_{\lambda_2}})$ and select the maximum point of λ_1 in the preimage of $\mathbf{\Lambda}$ as $\mathbf{v}_{\max \lambda_1} = (v_{p_{\max \lambda_1}}, v_{p_{\lambda_2}})$. The midpoint of the two points is:

$$\mathbf{v}_{\lambda_1} = \frac{1}{2}\left(\mathbf{v}_{\min \lambda_1} + \mathbf{v}_{\max \lambda_1}\right), \quad \zeta = \frac{1}{2} \tag{30}$$

Select the minimum point of λ_2 in the preimage of $\mathbf{\Lambda}$ as $\mathbf{v}_{\min \lambda_2} = (v_{p_{\lambda_1}}, v_{p_{\min \lambda_2}})$ and select the maximum point of λ_2 in the preimage of $\mathbf{\Lambda}$ as $\mathbf{v}_{\max \lambda_2} = (v_{p_{\lambda_1}}, v_{p_{\max \lambda_2}})$. The midpoint of the two points is:

$$\mathbf{v}_{\lambda_2} = \frac{1}{2}\left(\mathbf{v}_{\min \lambda_2} + \mathbf{v}_{\max \lambda_2}\right), \quad \zeta = \frac{1}{2} \tag{31}$$

According to the convex optimization theory, the median value is taken third times, and the median point must be inside the feasible polygon and away from the polygon boundary. Finally, the feasible point is determined:

$$\mathbf{v}_{\lambda} = \frac{1}{2}\left(\mathbf{v}_{\lambda_1} + \mathbf{v}_{\lambda_2}\right), \quad \zeta = \frac{1}{2} \tag{32}$$

Note that these formulas are applicable since we have found the full feasible polygon vertices. Finally, the desired feasible cable tension distribution point $\mathbf{v}_{\lambda}$ is determined after three centering and find $\mathbf{T} = \mathbf{T}_s + \mathbf{N}\mathbf{v}_{\lambda}$.

As Fig. 9 shown, the feasible point determined by the first centering is the midpoint of the black solid line marked with black triangle; The feasible point determined by the second centering is the midpoint of the red solid line marked red dot; The desired feasible point determined by the third centering is the midpoint of the purple solid line, marked with purple square. The flowchart of the proposed algorithm is shown in Fig. 10.

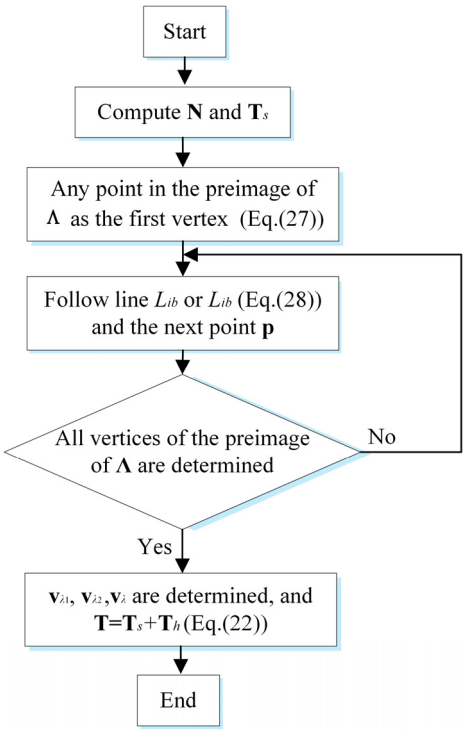

FIGURE 10. Flowchart of the algorithm of Section V.

C. PROOF OF CONTINUITY

If we prove that $\mathbf{T}$ is continuous, only need to prove that both $\mathbf{T}_s$ and $\mathbf{T}_h$ are continuous. Reference [34] has given the continuity proof of $\mathbf{T}_s$. It is no longer proved here that we only need to prove that $\mathbf{T}_h$ is continuous. The derivation process is as follows:

$$\mathbf{T}_h = \mathbf{N}\mathbf{v}_{\lambda} \tag{33}$$

Suppose that $\mathbf{v} = f(x)$ is a convex function, $[v_1, v_2] \in \mathbf{S}$, letting $M = \max\{f(v_1), f(v_2)\}$ and $x \in [v_1, v_2]$, it then

follows that:

$$f(x) = \zeta f(v_1) + (1-\zeta) f(v_2) \le \zeta M + (1-\zeta) M = M \tag{34}$$

Letting $x = \frac{v_1+v_2}{2} + \vartheta$, according to the convexity of the function $f(x)$, it can be obtained:

$$f(x) = f(\frac{v_1+v_2}{2} + \vartheta) \ge 2f(\frac{v_1+v_2}{2}) - f(\frac{v_1+v_2}{2} - \vartheta) \tag{35}$$

According to Eq. (34), it can be obtained:

$$f(x)) \ge 2f(\frac{v_1+v_2}{2}) - M = \mu \tag{36}$$

Letting $h > 0$, $[v_1 - h, v_2 + h] \in \mathbf{S}$, $x, y \in [v_1, v_2]$, suppose that $z = y + \frac{h}{|y-x|}(y-x)$, $\zeta = \frac{|y-x|}{h+|y-x|}$, so $z \in [v_1 - h, v_2 + h]$, $y = \zeta z + (1-\zeta)x$, it then follows that:

$$f(y) - f(x) < \zeta [f(z) - f(x)] \le \zeta (M - \vartheta) \tag{37}$$

Because $\zeta = \frac{|y-x|}{h+|y-x|} \le \frac{|y-x|}{h}$, it then follows that:

$$f(y) - f(x) < \frac{|y-x|}{h}(M - \vartheta) = K|y-x| \tag{38}$$

So the continuity of $\mathbf{v}$ is proved, and then $\mathbf{T}_h$ is continuous. Thus the continuity condition of $\mathbf{T}$ is proved.

VI. SIMULATION EXPERIMENTS

A simulation experiment of a 6-DOF 8 cable CDPR is carried out to verify the proposed rapid optimization algorithm of cable tension. Because the hinge position of the CDAVOTR's cable and the mobile platform can be flexibly changed, the simulation adopted a layout scheme 2 with larger workspace and pose angle. Set the mobile platform quality is 40 kg, the Euler angles (0°, 0°, 0°), when the mobile platform moves, the external force has gravity only.

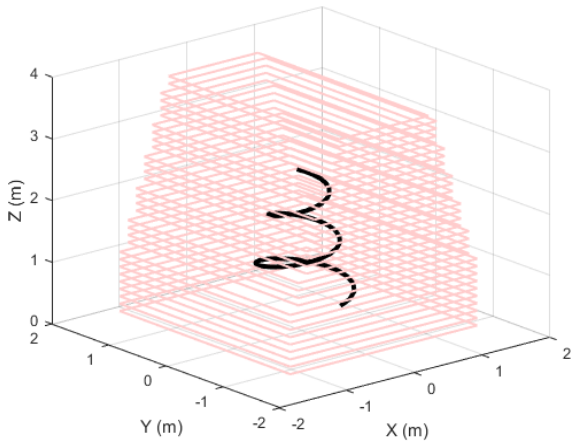

FIGURE 11. Spiral trajectory in the WFW.

The CDVATR tension optimization distribution process is implemented in MATLAB software. The trajectory of the desired motion of the mobile platform in the WFW is shown in Fig. 11. The red solid line is the robot WFW boundary, and the black solid line is the moving trajectory of the mobile platform. This trajectory is described as:

$$\begin{cases} X = \rho \times e^{-0.5wt} \times \cos(wt) \\ Y = \rho \times e^{-0.5wt} \times \sin(wt) \\ Z = vt + 0.6 \end{cases} \tag{39}$$

where ρ is the maximum radius of the spiral, w is the angular velocity of the mobile platform, v is the mobile platform Z direction speed, and t is trajectory time. The simulation used values of $\rho = 0.8$ m, $w = 0.8$ rad/s, $v = 1$ m/s, $t = 0{:}\ \pi/80{:}0.8\pi$. The starting point and pose of the mobile platform track are (0.055, −0.627, 0.6, 0°, 0°, 0°), termination point and pose are (0.152, 0.254, 2.485, 0°, 0°, 0°).

The experimental results shown in Fig. 12(a) illustrate the continuity of the proposed optimization algorithm. When (CDAVOTR) moves along the trajectory, the cable tensions vary continuously. According to the spiral trajectory (Fig. 11), the center of mass termination point of the mobile platform is 1.885 m higher than the starting point, and the angle between the cables 1-4 and the Z-axis increases with the height of the mobile platform. Therefore, the cable tension must be increased to balance the gravity of the mobile platform and the downward cable tension of cables 5-8. The angle between the cables 5-8 and the Z-axis decreases with the increase of the height of mobile platform, so the cable tension decreases gradually. Therefore, the cable tension of cables 1-4 at the trajectory termination point is greater than that at the starting point, and the cable tension at the track termination point of cables 5-8 is less than that at the starting point. The results show that the optimal tension distribution algorithm is continuous and feasible. In addition, Fig. 12(b) shows that the length of each cable varies continuously; the mobile platform raise, the cables 1-4 shortens, and cables 5-8 extends. From Fig. 12 (c), the speed change of each cable is a sine wave with decreasing amplitude, and the change process is continuous. When the mobile platform is located at a certain height, the greater the angle between the cables 1-4 and the Z-axis, the longer the cable, and the greater the cable tension should be to balance the gravity of the mobile platform and other cable tension, while cables 5-8 are the opposite. Therefore, the cable tension of cables 1-4 should gradually enlarge, that of cables 5-8 becomes smaller, and the change of cable tension in Fig. 12(a) is consistent with the law, thus proving the correctness of the proposed algorithm.

In order to prove that the proposed tension distribution algorithm is done in real time, the time for each step of the tension computation is analyzed when the spiral trajectory is completed, as shown in Fig. 13.

From Fig. 13, it can be seen that the average time of the cable tension distribution computation is 2 ms and the maximum time is 5 ms, so this has proven that the proposed algorithm can operate in real-time.

In order to prove the superiority of the proposed algorithm, compared with the minimum norm method of [34] and the safety tension method of [37], the three methods carried out

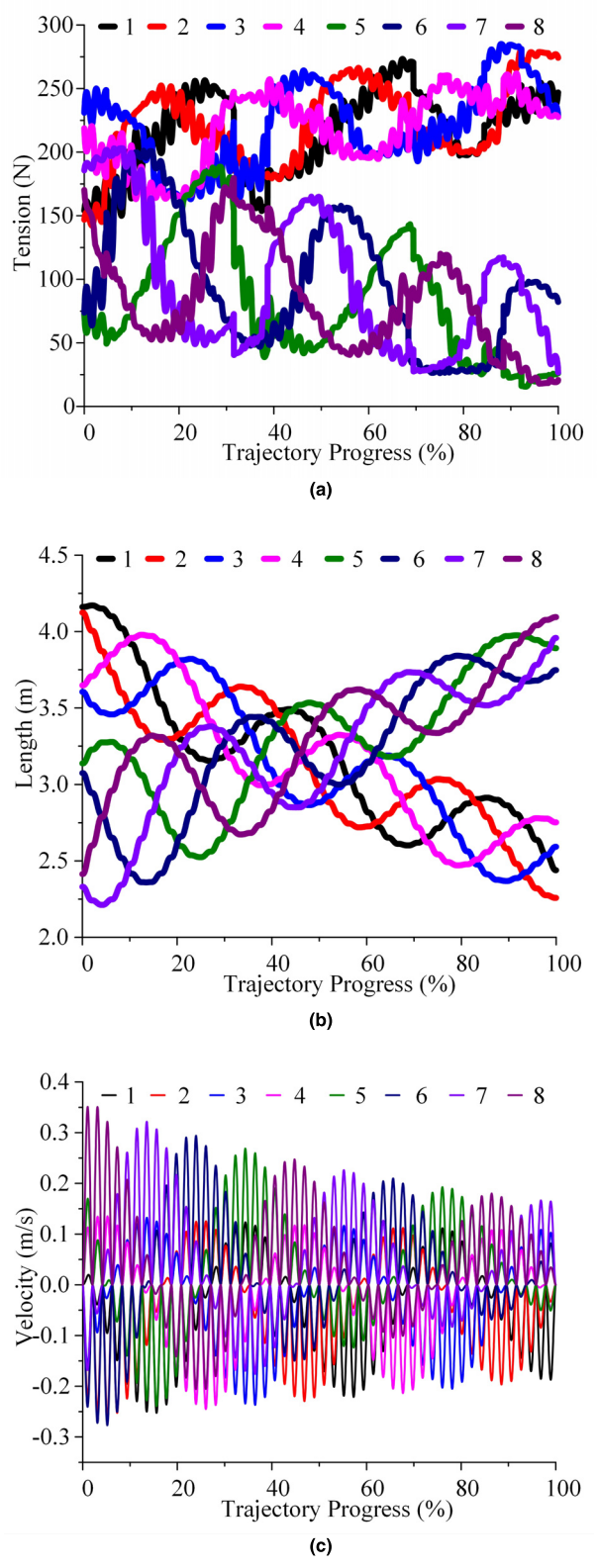

FIGURE 12. Proposed method results showing cable tension, cable length, cable velocity during execution of a spiral trajectory. (a) Tension distribution of proposed method. (b) Cable length. (c) Cable velocity.

the same spiral trajectory and the time taken for the tension distribution change when the mobile platform has different attitude angles is measured. Tension distribution of the two

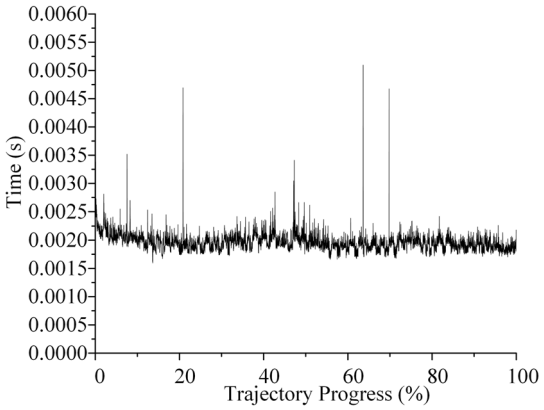

FIGURE 13. The computation time of proposed tension distribution method when the mobile platform moves along the spiral trajectory.

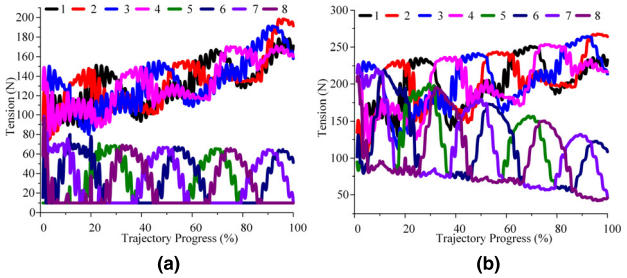

FIGURE 14. Tension distribution of (a) minimum norm method and (b) safety tension method when the mobile platform attitude angle is (0°, 0°, 0°).

methods from references when the mobile platform attitude angle is (0°, 0°, 0°) shown in Fig. 14. The all results are shown in Tables 3–5.

TABLE 3. Task execution time of three methods when the mobile platform attitude angle is (0°, 0°, 0°).

Method	MEAN	Standard deviation	total
Proposed method	0.0019 s	0.0004 s	9.3097 s
Minimum norm	0.0050 s	0.0009 s	23.8080 s
Safe tension	0.0070 s	0.0016 s	33.6872 s

TABLE 4. Task execution time of three methods when the mobile platform attitude angle is (3°, 0°, 0°).

Method	MEAN	Standard deviation	total
Proposed method	0.0019 s	0.0004 s	9.1062 s
Minimum norm	0.0050 s	0.0009 s	23.9746 s
Safe tension	0.0074 s	0.0119 s	35.4220 s

Obviously, when the mobile platform is in three different poses to complete the spiral trajectory, the proposed algorithm has the least cost and the standard deviation is the

TABLE 5. Task execution time of three methods when the mobile platform attitude angle is (3°, 1°, 3°).

Method	MEAN	Standard deviation	total
Proposed method	0.0020 s	0.0018 s	9.5802 s
Minimum norm	0.0052s	0.0179 s	25.1477 s
Safe tension	0.0071 s	0.0064 s	33.9314 s

smallest, and the total time spent on the whole trajectory is the shortest; The minimum norm method took less time than the safety tension method for the average time of tension distribution to complete the whole trajectory. Out of the three methods, the smaller the standard deviation of the computation time, the quicker the computation time, and therefore the greater the reliability of the real-time control.

Through the experimental results and comparative analysis, it is found that the proposed tension distribution method can operate in real-time and be continuous in the WFW.

VII. CONCLUSION

This paper has studied the key problems that need to be solved with regard to CDPRs real-time controls, including the WFW taking interference into consideration, and the configuration optimization and tension distribution. A WFW method of considering interference between cable and cable, and cable and the surface of the mobile platform has been proposed. It was possible to determine the workspace of the robot closer to the actual situation. The trajectory of the robot was controlled in this workspace.

The size of the mobile platform of the common cable parallel robots was optimized and the optimal size was also determined, which established the maximum WFW of the robot. The influence of the cable layout on the WFW was innovatively analyzed, and the cable layout was determined for the maximum workspace. The maximum attitude angle of the three layout schemes was determined, and the optimal scheme of the robot was determined by the comprehensive comparison.

In order to make the robot have real-time control in the WFW, a cable tension distribution method was proposed. This method can quickly determine the feasible point of tension distribution and reduce the time of the tension distribution computation. By comparing this with the results of two other algorithms, it was proven that the proposed algorithm is feasible and can operate in real-time.

REFERENCES

[1] M. Hassan and A. Khajepour, "Optimization of actuator forces in cable-based parallel manipulators using convex analysis," *IEEE Trans. Robot.*, vol. 24, no. 3, pp. 736–740, Jun. 2008.

[2] R. J. Caverly and J. R. Forbes, "Flexible cable-driven parallel manipulator control: Maintaining positive cable tensions," *IEEE Trans. Control Syst. Technol.*, to be published, doi: 10.1109/TCST.2017.2728007.

[3] G. Abbasnejad and M. Carricato, "Direct geometrico-static problem of underconstrained cable-driven parallel robots with *n* cables," *IEEE Trans. Robot.*, vol. 31, no. 2, pp. 468–478, Apr. 2015.

[4] Y. Mao and S. K. Agrawal, "Wearable cable-driven upper arm exoskeleton—Motion with transmitted joint force and moment minimization," in *Proc. IEEE Int. Conf. Robot. Automat.*, May 2010, pp. 4334–4339.

[5] G. Rosati, P. Gallina, and S. Masiero, "Design, implementation and clinical tests of a wire-based robot for neurorehabilitation," *IEEE Trans. Neural Syst. Rehabil. Eng.*, vol. 15, no. 4, pp. 560–569, Dec. 2007.

[6] X. Cui, W. Chen, X. Jin, and S. K. Agrawal, "Design of a 7-DOF cable-driven arm exoskeleton (CAREX-7) and a controller for dexterous motion training or assistance," *IEEE/ASME Trans. Mechatronics*, vol. 22, no. 1, pp. 161–172, Feb. 2017.

[7] J. P. Merlet and D. Daney, "A portable, modular parallel wire crane for rescue operations," in *Proc. IEEE Int. Conf. Robot. Automat.*, May 2010, pp. 2834–2839.

[8] R. Yao, X. Tang, J. Wang, and P. Huang, "Dimensional optimization design of the four-cable-driven parallel manipulator in FAST," *IEEE/ASME Trans. Mechatronics*, vol. 15, no. 6, pp. 932–941, Dec. 2010.

[9] B. Y. Duan, Y. Y. Qiu, F. S. Zhang, and B. Zi, "On design and experiment of the feed cable-suspended structure for super antenna," *Mechatronics*, vol. 19, no. 4, pp. 503–509, 2009.

[10] H. Li and R. Yao, "Optimal orientation planning and control deviation estimation on FAST cable-driven parallel robot," *Adv. Mech. Eng.*, vol. 6, p. 716097, Mar. 2014.

[11] A. Fortin-Côté, P. Cardou, and C. Gosselin, "An admittance control scheme for haptic interfaces based on cable-driven parallel mechanisms," in *Proc. IEEE Int. Conf. Robot. Automat. (ICRA)*, May/Jun. 2014, pp. 819–825.

[12] L. Dominjon, J. Perret, and A. Lécuyer, "Novel devices and interaction techniques for human-scale haptics," *Vis. Comput.*, vol. 23, no. 4, pp. 257–266, 2007.

[13] S. Perreault and C. M. Gosselin, "Cable-driven parallel mechanisms: Application to a locomotion interface," *J. Mech. Des.*, vol. 130, no. 10, p. 102301, 2008.

[14] B. Ouyang and W.-W. Shang, "A new computation method for the force-closure workspace of cable-driven parallel manipulators," *Robotica*, vol. 33, no. 3, pp. 537–547, 2015.

[15] J. P. Merlet, "Checking the cable configuration of cable-driven parallel robots on a trajectory," in *Proc. IEEE Int. Conf. Robot. Automat.*, May/Jun. 2017, pp. 1586–1591.

[16] R. Verhoeven, "Analysis of the workspace of tendon-based stewart platforms," M.S. thesis, Dept. Von der Fakultät Ingenieurwissenschaften, Univ. Duisburg-Essen, Duisburg, Germany, 2004.

[17] C. B. Pham, S. H. Yeo, G. Yang, M. S. Kurbanhusen, and I. M. Chen, "Force-closure workspace analysis of cable-driven parallel mechanisms," *Mech. Mach. Theory*, vol. 41, no. 1, pp. 53–69, 2006.

[18] X. M. Diao and O. Ma, "Workspace analysis of a 6-DOF cable robot for hardware-in-the-loop dynamic simulation," in *Proc. IEEE Int. Conf. Intell. Robots Syst.*, Oct. 2006, pp. 4103–4108.

[19] M. Gouttefarde, D. Daney, and J.-P. Merlet, "Interval-analysis-based determination of the wrench-feasible workspace of parallel cable-driven robots," *IEEE Trans. Robot*, vol. 27, no. 1, pp. 1–13, Feb. 2011.

[20] M. Gouttefarde, J.-P. Merlet, and D. Daney, "Wrench-feasible workspace of parallel cable-driven mechanisms," in *Proc. IEEE Int. Conf. Robot. Automat.*, Apr. 2007, pp. 1492–1497.

[21] Q. Duan, V. Vashista, and S. K. Agrawal, "Effect on wrench-feasible workspace of cable-driven parallel robots by adding springs," *Mech. Mach. Theory*, vol. 86, pp. 201–210, Apr. 2015.

[22] I. Ebert-Uphoff and P. A. Voglewede, "On the connections between cable-driven robots, parallel manipulators and grasping," in *Proc. IEEE Int. Conf. Robot. Automat.*, Apr./May 2004, pp. 4521–4526.

[23] P. Bosscher, A. T. Riechel, and I. Ebert-Uphoff, "Wrench-feasible workspace generation for cable-driven robots," *IEEE Trans. Robot.*, vol. 22, no. 5, pp. 890–902, Oct. 2006.

[24] J.-P. Merlet, "Analysis of the influence of wires interference on the workspace of wire robots," in *Proc. 9th Int. Symp. Adv. Robot Kinematics*. Dordrecht, The Netherlands: Springer, Jun. 2004, pp. 211–218.

[25] L. Blanchet and J.-P. Merlet, "Interference detection for cable-driven parallel robots (CDPRs)," in *Proc. IEEE/ASME Int. Conf. Adv. Intell. Mechatronics (AIM)*, Jul. 2014, pp. 1413–1418.

[26] Y. Wischnitzer, N. Shvalb, and M. Shoham, "Wire-driven parallel robot: Permitting collisions between wires," *Int. J. Robot. Res.*, vol. 27, no. 9, pp. 1007–1026, 2008.

[27] G. Rosati, D. Zanotto, and S. K. Agrawal, "On the design of adaptive cable-driven systems," *J. Mech. Robot.*, vol. 3, no. 2, p. 021004, 2011.

[28] D. Zanotto, G. Rosati, S. Minto, and A. Rossi, "Sophia-3: A semiadaptive cable-driven rehabilitation device with a tilting working plane," *IEEE Trans. Robot.*, vol. 30, no. 4, pp. 974–979, Aug. 2014.
[29] S. Abdolshah, D. Zanotto, G. Rosati, and S. K. Agrawal, "Optimizing stiffness and dexterity of planar adaptive cable-driven parallel robots," *J. Mech. Robot.*, vol. 9, no. 3, p. 031004, 2017.
[30] D. Q. Nguyen, M. Gouttefarde, O. Company, and F. Pierrot, "On the analysis of large-dimension reconfigurable suspended cable-driven parallel robots," in *Proc. IEEE Int. Conf. Robot. Automat. (ICRA)*, May/Jun. 2014, pp. 5728–5735.
[31] D. Q. Nguyen and M. Gouttefarde, "Study of reconfigurable suspended cable-driven parallel robots for airplane maintenance," in *Proc. IEEE/RSJ Int. Conf. Intell. Robots Syst. (IROS)*, Sep. 2014, pp. 1682–1689.
[32] L. Gagliardini, S. Caro, M. Gouttefarde, and A. Girin, "A reconfiguration strategy for reconfigurable cable-driven parallel robots," in *Proc. IEEE Int. Conf. Robot. Automat. (ICRA)*, May 2015, pp. 1613–1620.
[33] H. Jamshidifar, A. Khajepour, B. Fidan, and M. Rushton, "Kinematically-constrained redundant cable-driven parallel robots: Modeling, redundancy analysis, and stiffness optimization," *IEEE/ASME Trans. Mechatronics*, vol. 22, no. 2, pp. 921–930, Apr. 2017.
[34] Y. Su, Y. Qiu, and P. Liu, "The continuity and real-time performance of the cable tension determining for a suspend cable-driven parallel camera robot," *Adv. Robot.*, vol. 29, no. 12, pp. 743–752, 2015.
[35] P. H. Borgstrom *et al.*, "NIMS-PL: A cable-driven robot with self-calibration capabilities," *IEEE Trans. Robot.*, vol. 25, no. 5, pp. 1005–1015, Oct. 2009.
[36] K. Müller, C. Reichert, and T. Bruckmann, "Analysis of a real-time capable cable force computation method," in *Proc. 2nd Int. Conf. Cable-Driven Parallel Robots*, vol. 41, no. 20. Berlin, Germany: Springer-Verlag, 2015, pp. 227–238.
[37] P. H. Borgstrom, B. L. Jordan, G. S. Sukhatme, M. A. Batalin, and W. J. Kaiser, "Rapid computation of optimally safe tension distributions for parallel cable-driven robots," *IEEE Trans. Robot.*, vol. 25, no. 6, pp. 1271–1281, Dec. 2009.
[38] L. Mikelsons, T. Bruckmann, M. Hiller, and D. Schramm, "A real-time capable force calculation algorithm for redundant tendon-based parallel manipulators," in *Proc. IEEE Int. Conf. Robot. Automat.*, May 2008, pp. 3869–3874.
[39] T. Bruckmann, L. Mikelsons, M. Hiller, and D. Schramm, "A new force calculation algorithm for tendon-based parallel manipulators," in *Proc. IEEE/ASME Int. Conf. Adv. Intell. Mechatronics*, Sep. 2007, pp. 1–6.
[40] M. Gouttefarde, J. Lamaury, C. Reichert, and T. Bruckmann, "A versatile tension distribution algorithm for n-DOF parallel robots driven by $n+2$ cables," *IEEE Trans. Robot.*, vol. 31, no. 6, pp. 1444–1457, Dec. 2015.
[41] B. Ouyang and W. Shang, "Wrench-feasible workspace based optimization of the fixed and moving platforms for cable-driven parallel manipulators," *Robot. Comput.-Integr. Manuf.*, vol. 30, no. 6, pp. 629–635, 2014.
[42] S. Bouchard, C. Gosselin, and B. Moore, "On the ability of a cable-driven robot to generate a prescribed set of wrenches," *J. Mech. Robot.*, vol. 2, no. 1, p. 011010, 2010.
[43] S. Tadokoro, Y. Murao, M. Hiller, R. Murata, H. Kohkawa, and T. Matsushima, "A motion base with 6-DOF by parallel cable drive architecture," *IEEE/ASME Trans. Mechatronics*, vol. 7, no. 2, pp. 115–123, Jun. 2002.
[44] H. Yuan, E. Courteille, M. Gouttefarde, and P.-E. Hervé, "Vibration analysis of cable-driven parallel robots based on the dynamic stiffness matrix method," *J. Sound Vib.*, vol. 394, pp. 527–544, Apr. 2017.
[45] A. Pott, H. Mütherich, W. Kraus, V. Schmidt, P. Miermeister, and A. Verl, "IPAnema: A family of cable-driven parallel robots for industrial applications," *Mech. Mach. Sci.*, vol. 12, pp. 119–134, 2013, doi: 10.1007/978-3-642-31988-4_8.
[46] W. B. Lim, G. Yang, S. H. Yeo, S. K. Mustafa, and I.-M. Chen, "A generic tension-closure analysis method for fully-constrained cable-driven parallel manipulators," in *Proc. IEEE Int. Conf. Robot. Automat. (ICRA)*, May 2009, pp. 2187–2192.
[47] W. B. Lim, G. Yang, S. H. Yeo, and S. K. Mustafa, "A generic force-closure analysis algorithm for cable-driven parallel manipulators," *Mech. Mach. Theory*, vol. 46, no. 9, pp. 1265–1275, 2011.
[48] D. Lau, J. Eden, Y. Tan, and D. Oetomo, "CASPR: A comprehensive cable-robot analysis and simulation platform for the research of cable-driven parallel robots," in *Proc. IEEE Int. Conf. Intell. Robots Syst.*, Oct. 2016, pp. 3004–3011.
[49] M. Hiller, S. Fang, S. Mielczarek, R. Verhoeven, and D. Franitza, "Design, analysis and realization of tendon-based parallel manipulators," *Mech. Mach. Theory*, vol. 40, no. 4, pp. 429–445, 2005.
[50] J. Lamaury and M. Gouttefarde, "A tension distribution method with improved computational efficiency," in *Proc. Int. Conf. Cable-Driven Parallel Robots*, 2013, pp. 71–85.
[51] J. Lamaury and M. Gouttefarde, "Control of a large redundantly actuated cable-suspended parallel robot," in *Proc. IEEE Int. Conf. Robot. Automat.*, May 2013, pp. 4659–4664.

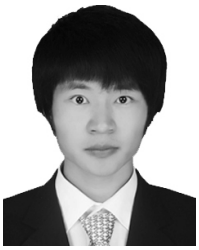

DA SONG was born in Chifeng, China, in 1989. He received the B.S. degree in mechanical design and automation from Hulunbuir University, Hulunbuir, China, in 2012, and the M.S. degree in mechanical engineering from Harbin Engineering University, Harbin, China, in 2015, where he is currently pursuing the Ph.D. degree with the College of Mechanical and Electrical Engineering. His main research interests are parallel robot and robot technology.

LIXUN ZHANG was born in Yingkou, China, in 1962. He received the B.S. and M.S. degrees from the College of Mechanical and Electrical Engineering, Harbin Engineering University, Harbin, China, and the Ph.D. degree from the Harbin Institute of Technology, Harbin, in 1994. He is currently a Professor and a Doctoral Advisor with the College of Mechanical and Electrical Engineering, Harbin Engineering University. His main research interests are parallel robot, rehabilitation robot, robot technology, and cobot.

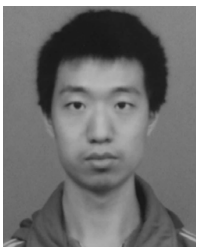

FENG XUE was born in Shijiazhuang, China, in 1992. He received the B.S. degree in mechanical design and automation and the M.S. degree in mechanical engineering from Harbin Engineering University, Harbin, China, in 2015 and 2017, respectively, where he is currently pursuing the Ph.D. degree with the College of Mechanical and Electrical Engineering. His main research interests are parallel robot and machine learning.